Korean J. Chem. Eng., 33(4), 1153-1158 (2016)
DOI: 10.1007/s11814-015-0226-4

pISSN: 0256-1115
eISSN: 1975-7220

Modeling and analysis of circulation variables of continuous sorbent loop cycling for CO_2 capture

Kee-Youn Yoo*, Jun-Soo Park, and Myung-June Park**,***,†**

*Department of Chemical and Biomolecular Engineering, Seoul National University of Science and Technology, Seoul 01811, Korea
**Department of Energy Systems Research, Ajou University, Suwon 16499, Korea
***Department of Chemical Engineering, Ajou University, Suwon 16499, Korea
(*Received 17 August 2015 • accepted 26 October 2015*)

Abstract−Carbon capture and storage (CCS) technologies are a cornerstone for reducing CO_2 emissions from energy and energy-intensive industries. Among the various CCS technologies, solid sorbent looping systems are considered to be potentially promising solutions for reducing CO_2 capture energy penalty. We present an evaluation module for a carbonator with sorbent looping cycle to calculate the carbonation efficiency. The module incorporates a simple sorbent activity model, and the solid/gas balances are constructed by assuming simple reactor mixing quality. By conducting simulations, we examine the variation in the carbonation efficiencies as a function of the sorbent looping operation factors and discuss an optimum operating strategy.

Keywords: Continuous Loop Carbonator, CO_2 Capture, Partial Least Square Parameterization

INTRODUCTION

Carbon capture and storage (CCS) is an important mitigation technology for reducing anthropogenic CO_2 emissions from industrial and energy-related point sources [1]. Several technologies for CO_2 capture including amine scrubbing, ammonia scrubbing, oxy-combustion, anti-sublimation, calcium looping, and indirect calcination have received great attention. Among these, one of the most promising technologies from an industrial point of view is the adsorption process based on the reversible reaction of CO_2 on specific metal oxides at high temperatures. CaO-based sorbents have attracted the most attention owing to their high absorption capacity, wide availability, and low cost. In addition, a state-of-the-art circulating fluidized bed (CFB) system, used in post-combustion calcium looping processes, offers relatively small energy penalty [2,3] since it provides high heat transfer, uniform and controllable temperature profiles, favorable gas-solid contacting, and the ability to handle wide variations in particulate properties [4]. A typical CFB system involves two reactors: the carbonator and calciner or regenerator. In the first reactor (carbonator), CO_2 reacts with CaO particulates to form limestone ($CaCO_3$), while sorbent regeneration and release of CO_2 take place in the second reactor (calciner or regenerator). The calcination reaction is strongly endothermic and occurs at temperatures above 900 °C achieved by fuel combustion in the calciner. Pure O_2 stream is used as an oxidizing agent to achieve high CO_2 concentrations in the exit gas. On the contrary, the carbonation reaction is exothermic and is realized at lower temperatures of 600-700 °C [5].

†To whom correspondence should be addressed.
E-mail: mjpark@ajou.ac.kr

There are many reports on modeling approaches for describing the carbon-capture technology, among which the 1-D fluidized bed model has been widely used [6,7]. Fang et al. [8] determined the kinetic rate constants for calcium looping cycles and developed a mathematical model. Wang et al. [9] proposed that dynamic and cyclic steam injection were favorable for preventing the sintering of modified CaO-based sorbents and facilitating diffusion. Hejazi et al. [10] evaluated the effects of key process variables such as temperature, pressure, and solids circulation rate on the steam gasification of biomass. Sarkar et al. [11] conducted multiphase computational fluid dynamic (CFD) simulations for the regenerator, besides applying CFD for both the reactors with focus on the flow characteristics [12,13].

In the area of reactor modeling, Kunii and Levenspiel [14,15] developed the K-L model to explain and correlate the observed reaction rate with physio-chemical phenomena occurring in the fluidized beds. They considered gas-solid mass transfer, gas-solid heat transfer, and solid catalyzed chemical reactions as factors influencing the rate. The model has been extensively used to fit reactivity data from laboratory tests of sorbent deactivation [16]. Meanwhile, there are several reports where simple and empirical reactor models have been used to describe the apparent kinetics of CaO carbonation [17,18].

Previously, we developed a partial least square (PLS)-based sorbent activity model for a carbonator under batch operation mode [19]. Since the sorbent activity is affected by the regeneration cycle number, reactor temperature, and particle size, two design parameters for the particle activity model, namely the characteristic time (t*) and maximum attainable conversion of particles (X_N), were determined as functions of the carbonator operating conditions by applying the PLS method to experimental data reported in the literature [17,19]. In the present work, we have developed an evalua-

tion module for a carbonator with continuous sorbent looping by incorporating the PLS-based activity model to calculate the CO_2 capture efficiency. The carbonator evaluation module is based on solid and gas balances with the effective average residence time used as an adjustable parameter. By applying the evaluation module, we obtain the carbonation efficiencies as a function of the circulation operation factors and are able to suggest an optimal operating strategy.

MATHEMATICAL MODELING

1. PLS-based Carbonation Reaction Model

In commercial-scale carbonators, a carbonation reaction occurs in the fast kinetic-controlled regime, which is followed by a very slow CO_2 diffusion-controlled regime [16]. When the contact time (t) between the solid absorbent and CO_2 is lower than t*, the reaction occurs at a nearly constant rate. The reaction is extinguished after t* as described in Eq. (1) [16,19]:

$$r_{CaO}=\begin{cases}\dfrac{X_N}{t^*} & \text{for } t<t^*\\ 0 & \text{for } t>t^*\end{cases} \tag{1}$$

where X_N represents the maximum attainable conversion of particles in the N^{th} cycle, and usually decreases with increasing cycle numbers. Since the sorbent activity is observed to vary with the regeneration cycle number, reactor temperature, and particle size, two key parameters for the particle activity model, namely t* and X_N, were determined as functions of the carbonator operating conditions by applying the PLS method [19] to the experimental data reported in the literature [17]. The cycle number (N), temperature (T), and particle diameter (d_p) were studied as manipulated variables (x_i), and they were correlated with t* and X_N. Nonlinear terms were included in the input vector to address the nonlinearity of the relationship as follows (Eq. (2)).

$$\mathbf{x}^T=[x_i,\ x_i^2,\ x_i x_{j\neq i},\ \ln x_i],\ (i, j=N, T, d_p) \tag{2}$$

Finally, a prediction model for quality variables ($\mathbf{y}=[t^*\ X_N]$) was constructed by applying the PLS algorithm in the linear regression form as follows (Eq. (3); *cf.* Table 2 in [19] for detailed values).

$$\hat{\mathbf{y}}_h=\mathbf{x}^T\hat{\mathbf{b}} \tag{3}$$

2. Continuous Carbonator Model

Eq. (1) allows the calculation of the carbonation rate of an absorbent particle that is progressing towards X_N given by Eq. (3) as a function of the operating conditions, especially the number of cycles (N). However, in the presence of circulating particle streams, i.e., the continuous feed of fresh particles and purging of aged ones in the carbonator-calciner loop system shown in Fig. 1, a mixture of particles with different cycle numbers and different activities for CO_2 capture (depending on N) will exist in the carbonator. Assuming that the solid particles are perfectly mixed in both the beds, it is possible to calculate the inlet flow rates of the k^{th} generated particles (F_k) into the carbonator and the fraction of active particles ($f_{a,k}$) corresponding to the k^{th} generated particles that have not yet fully reached their maximum attainable conversion (X_N^k) as follows:

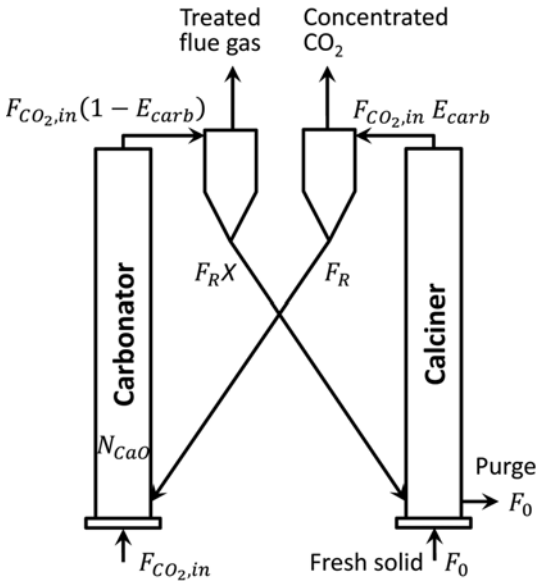

Fig. 1. Scheme of the continuous carbonator with sorbent looping cycle. The amounts of CO_2 in the treated flue gas and concentrated CO_2 streams are $F_{CO_2,in}(1-E_{carb})$ and $F_{CO_2,in}E_{carb}$, respectively, and their sum is equal to $F_{CO_2,in}$ to satisfy overall mass balance.

$$F_k=F_0R_F^k,\ R_F=\frac{F_R}{F_R+F_0},\ k=1, 2, 3\cdots \tag{4}$$

$$f_{a,k}=1-\exp(-t_k^*/\tau) \tag{5}$$

where F_R and F_0 denote the overall inlet flow rate of particles into the carbonator and make-up rate of fresh particles into the calciner, respectively, and τ is the average particle residence time in the carbonator. τ is defined by Eq. (6).

$$\tau=\frac{W_{CaO}}{M_{CaO}F_R} \tag{6}$$

The various symbols in the equation are defined in the Nomenclature section.

Considering the PLS-based simple reaction model, the carbonates leaving the carbonator at the steady state have two contributions from carbonates converted to their maximum attainable conversions ($X_{N,k}$) depending on the individual cycle number (k) in the extinguished particles whose contact time (t) is higher than t_k^* and active particles with contact time (t) lower than t_k^* still reacting at the carbonation rate given by Eq. (1). Incorporating these two contributions, the conversion is calculated as follows (Eq. (7)):

$$F_RX=\Sigma_{k=1}^{\infty}F_k(f_{a,k}\overline{X}_k+(1-f_{a,k})X_{N,k}) \tag{7}$$

where $\overline{X}_k$ represents the average conversion of the k^{th} regenerated active particle with a contact time (t) lower than t_k^*, and is calculated by Eq. (8).

$$\overline{X}_k=\frac{1}{f_{a,k}}\int_0^{t_k^*}r_{CaO,k}\frac{t}{\tau}\exp\left(-\frac{t}{\tau}\right)dt \tag{8}$$

Using Eqs. (1) and (5) for $r_{CaO,k}$ and t_k^*, respectively, the average conversion of the k^{th} regenerated lime particles in the carbonator is

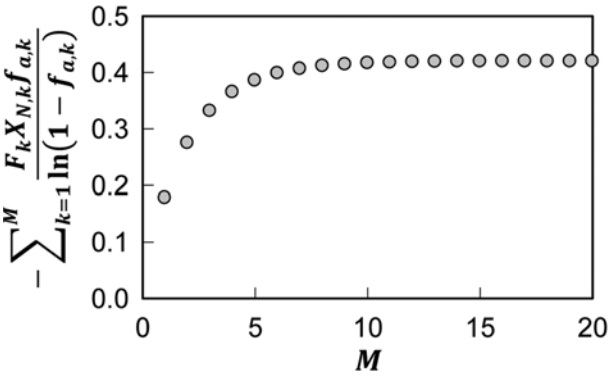

Fig. 2. Convergence of the partial sums of the infinite series in Eq. (10) (carbon solid balance).

derived as a function of the fractions of active particles ($f_{a,k}$) as follows (Eq. (9)).

$$\overline{X}_k = X_{N,k}\left[\left(1-\frac{1}{f_{a,k}}\right)-\frac{1}{\ln(1-f_{a,k})}\right] \quad (9)$$

Substituting Eq. (9) into Eq. (7) results in the following equation (Eq. (10)) for the average conversion of the solids leaving the carbonator (X).

$$X = -\frac{1}{F_R}\Sigma_{k=1}^{\infty} F_k X_{N,k}\frac{f_{a,k}}{\ln(1-f_{a,k})} \quad (10)$$

The ratio test shows that the infinite series in Eq. (10) is always convergent.

$$\lim_{k\to\infty}\frac{F_{k+1}X_{N,k+1}f_{a,k+1}/\ln(1-f_{a,k+1})}{F_k X_{N,k} f_{a,k}/\ln(1-f_{a,k})} \approx R_F < 1 \quad (11)$$

Fig. 2 shows that the partial sums of the infinite series in Eq. (10) converge rapidly within 20 terms under typical operating conditions. As a result, the carbon capture efficiency (E_{carb}) is calculated by substituting the PLS-correlated solid activity model (Eq. (3)) and Eq. (5) into the solid balance (Eq. (10)), as shown in Eq. (12).

$$E_{carb} = \frac{F_R}{F_{CO_2,in}}X \quad (12)$$

Alvarez and Abanades [20] reported that, for most types of limes and regeneration number (N), the conversion of solid particles reaches X_N when the gas-solid reaction front is at a distance of *ca.* 50 nm (ε_{max}) from the pore walls. Thus, the specific reaction surface area S_N can be deduced from X_N as follows:

$$S_N = \frac{X_N}{\varepsilon_{max}}\frac{\rho_{CaO}/M_{CaO}}{\rho_{CaCO_3}/M_{CaCO_3}} \quad (13)$$

Assuming that the fast reaction regime is dominated by the reaction control of CaO with CO_2, the following gas consumption rate is obtained:

$$r_{CO_2} = k_s S_N (C_{CO_2} - C_{CO_2,e}) \quad (14)$$

By combining Eqs. (5) and (13) depending on the PLS-correlated solid activity model and the gas consumption rate (Eq. (14)), the carbon mass balance in the gas phase can be written as follows:

$$F_{CO_2,in}\frac{dE_{carb}}{dz} = A\frac{\rho_{CaO}}{M_{CaO}}k_s\left(\Sigma_{k=1}^{\infty}\frac{F_k}{F_R}f_{a,k}S_{N,k}\right)C_{in}\left[f_{in}\left(\frac{1-E_{carb}}{1-f_{in}E_{carb}}\right)-f_e\right] \quad (15)$$

In the above equation, E_{carb} and $F_{CO_2,in}$ represent the capture efficiency and feed flow rate of CO_2 in the carbonator, respectively, and k_s, f_{in}, and C_{in} on the right-hand side of the equation denote the kinetic rate constant, molar fraction of CO_2, and feed CO_2 concentration at the inlet of the carbonator reactor, respectively. By using the above gas phase balance, it is possible to calculate the axial concentration profile of CO_2 in the carbonator.

Note that the exit carbonation efficiency in Eq. (15) should be equal to the carbonation efficiency calculated from the solid balance shown in Eq. (12). However, in some cases, those two values do not match, which is attributed to the simple assumptions made regarding the fluid dynamics of the gas (plug flow) and solid (instant and perfect mixing). When (1) the fraction of fresh catalyst is high (i.e., when there is a large amount of fresh sorbent with high activity) for a fixed F_R, (2) fraction of circulating flow rate is very high compared to F_0 (τ_{eff} and τ are low, resulting in high

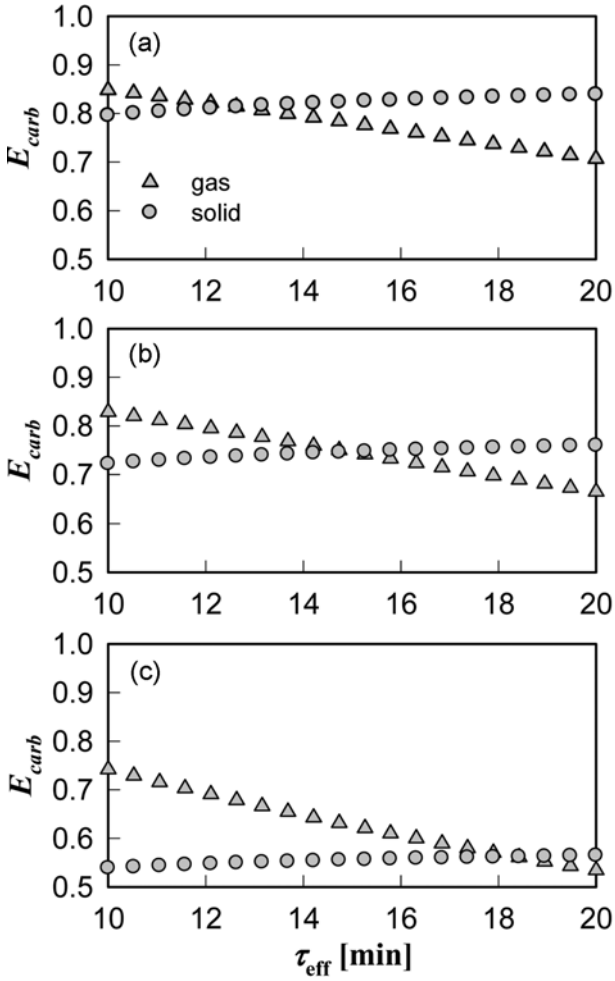

Fig. 3. Matching of the solid and gas balances with the effective average residence time under various solid looping conditions (T= 928 K, d_p=0.5 mm, F_R=10 mol/s, $F_{CO_2,in}$=5 mol/s, τ=20 min); (a) F_0=5 mol/s (R_F=0.67), (b) F_0=3 mol/s (R_F=0.77), and (c) F_0=1 mol/s (R_F=0.91).

activity as shown in Eq. (5)), and (3) CO_2 feed flow rate is low (gas residence time is very high), the CO_2 consumption rate is so high that the concentration reaches equilibrium even when the gas contact time is lower than t* and thus, the posterior section of the carbonator is under the stagnant regime. Thus, the carbonator bed is not completely used, indicating that the actual residence time is lower than τ. For example, Fig. 3 shows the carbonation efficiency at the exit when τ is fixed at 20 min and the fraction of F_R (R_F) is varied. Clearly, the efficiencies calculated from the gas and solid balances are different at τ=20, and the actual residence time (τ_{eff}), which is obtained from the intersection between the two balances, reaches a value close to τ with increasing R_F. This is because when the value of R_F is increased, the fraction of fresh catalyst is decreased, and thus, the CO_2 concentration is far from the equilibrium. We used the simple bisection algorithm to calculate the exact value of τ_{eff} with τ used as one of initial guesses (the other guess is specified arbitrarily). Finally, τ_{eff} is introduced into Eq. (5) as follows:

$$f_{a,k}=1-\exp(-t_k^*/\tau_{eff}) \quad (5)$$

RESULTS AND DISCUSSION

The continuous sorbent looping carbonator module with the PLS-correlated sorbent activity model was applied to operating conditions that are representative of the actual operation (a power plant delivering a given flow rate of CO_2, $F_{CO_2,in}$). As in the case of any fluidized bed, there is a need for a good knowledge of the fluid dynamics inside the carbonator to determine the solid content (W_{CaO}) and the gas-solid contact quality. However, it is beyond the scope of the present work to incorporate a detailed fluid dynamics sub-model into the carbonator module. Instead, the objective of this work was to determine the principal operating variables to economically achieve a given carbon capture efficiency.

1. Effects of Make-up Flow Rate F_0

Fig. 4 shows the variation in the effective average residence time and the exit carbonation efficiency as a function of the make-up flow rate. The exit carbonation efficiency approaches the maximum attainable value, and the effective average residence time decreases gradually when the make-up flow rate matches the solid circulation flow rate (F_R). When the make-up flow rate is close to one-half of the circulation flow rate (F_0=0.5F_R=5 mol/s), the carbonation efficiency is already close to the maximum value. In Fig. 5, variation in the axial carbonation efficiency is presented corresponding to the make-up flow rate in Fig. 4. Here, it is also observed that when the value of F_0 is high, the CO_2 concentration

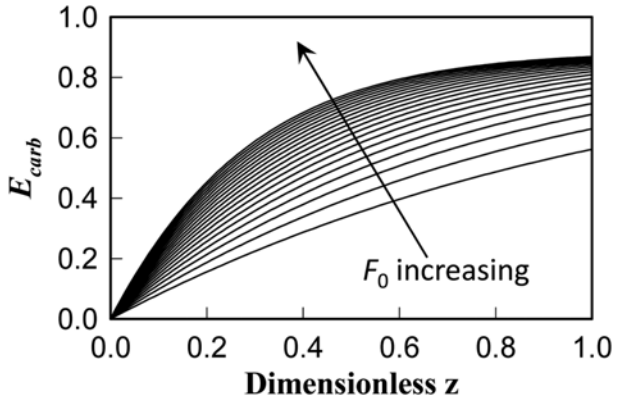

Fig. 5. Effects of make-up flow rate F_0 on the variation in axial carbonation efficiency (T=928 K, d_p=0.5 mm, F_R=10 mol/s, $F_{CO_2,in}$=5 mol/s, N_{CaO}=20 kmol).

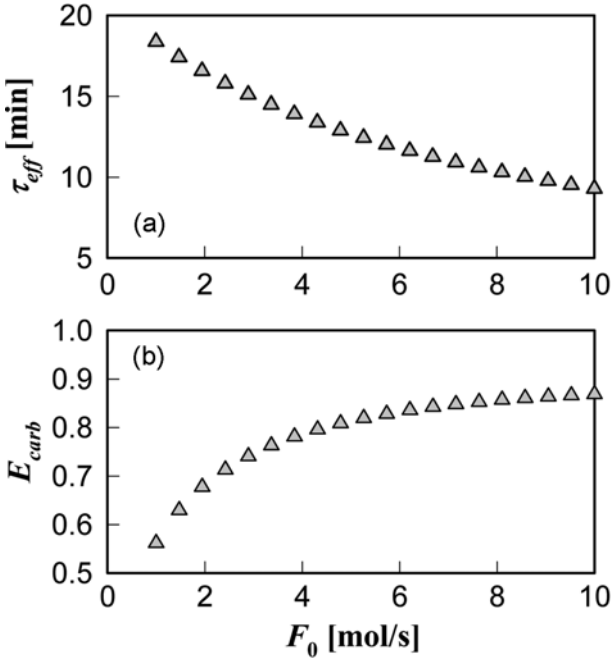

Fig. 4. Effects of make-up flow rate F_0 on the effective average residence time and the carbonation efficiency (T=928 K, d_p=0.5 mm, F_R=10 mol/s, $F_{CO_2,in}$=5 mol/s, τ=20 min).

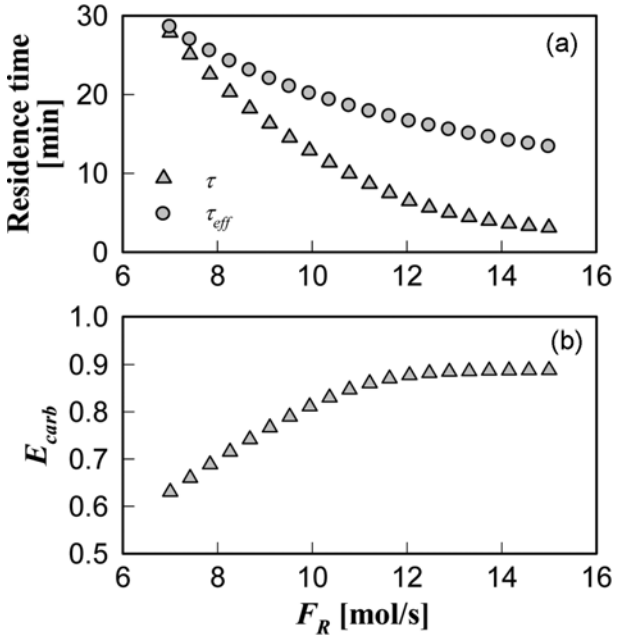

Fig. 6. Effects of circulation flow rate R_F on the effective average residence time and the carbonation efficiency (T=928 K, d_p=0.5 mm, F_0=5 mol/s, $F_{CO_2,in}$=5 mol/s, N_{CaO}=20 kmol).

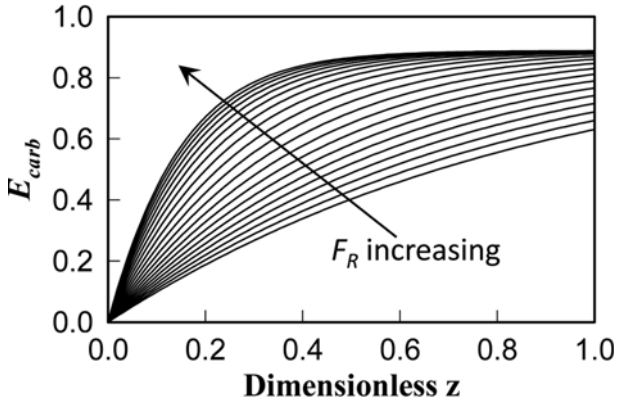

Fig. 7. Effects of circulation flow rate R_F on the variation in axial carbonation efficiency (T=928 K, d_p=0.5 mm, F_0=5 mol/s, $F_{CO_2,in}$=5 mol/s, τ=20 min).

reaches equilibrium rapidly and the reaction is stagnant in the rear section. As a result, the effective average residence time is reduced significantly compared to the actual residence time.

2. Effects of Circulation Flow Rate F_R

Figs. 6 and 7 provide results similar to Figs. 4 and 5, except that the former shows the variation in the circulation flow rate instead of the make-up flow rate. The average residence time also reduces linearly depending on the circulation flow rate and, at high circulation rates, the effective average residence time and average residence time exhibit similar decreasing slopes. Further increase in the circulation rate leads the reaction into the stagnant regime (Fig. 7) (see the discussion in section 2: Continuous carbonator model in the MATHEMATICAL MODELING section).

3. Effects of Carbonator CaO Holding

Carbonator holding weight of CaO (W_{CaO}) is mainly determined to guarantee the fluidization of solid particles and is also depending on a given flow rate of CO_2 ($F_{CO_2,in}$). In the present work, the reference value of N_{CaO} (number of moles of CaO) was selected using the reported value [21]. Fig. 8 shows the effects of two sorbent looping reactor operating factors, F_0 and F_R with different CaO holding weights on the exit carbonation efficiency. The sorbent holding weight mainly determined by the fluidization technology affects the maximum attainable value of the exit carbonation efficiency. In particular, the maximum attainable values are achieved over the wide range of solid flow rates. Therefore, we deduce that the optimum operating conditions would occur at the boundary of the flat surfaces (red surfaces in Fig. 8) of the maximum attainable value to minimize the operating costs at maximum efficiency.

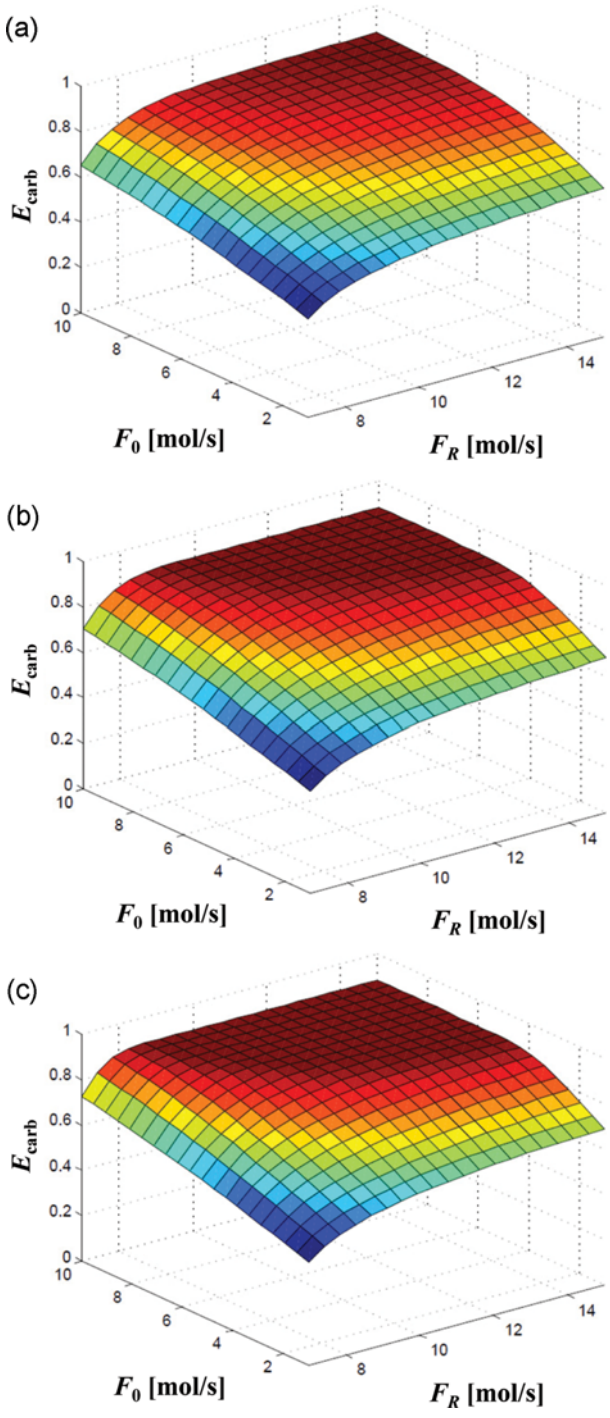

Fig. 8. Effects of sorbent holding N_{CaO} in the carbonator on the carbonation efficiency (a) N_{CaO}=10 kmol, (b) N_{CaO}=20 kmol, (c) N_{CaO}=30 kmol (T=928 K, d_p=0.5 mm, $F_{CO_2,in}$=5 mol/s).

CONCLUSIONS

We developed an evaluation module to study the optimal design and operation of a carbonator for CO_2 capture with a continuous sorbent loop cycle. The carbonator model was constructed by combining the solid and gas balances with the PLS-based sorbent activity model under simple kinetic assumption. Simulation studies confirmed that more than 85% carbonation efficiencies are achievable over a wide range of two main operation factors, F_0 and F_R, by applying continuous sorbent looping. Also, the maximum carbon capture efficiency with the reduced operating cost can be retained if these operation factors are selected at the boundary of the flat regime of maximum obtainable efficiencies.

ACKNOWLEDGEMENTS

This work was supported by the Energy Efficiency & Resources

Core Technology Program of the Korea Institute of Energy Technology Evaluation and Planning (KETEP) financed by the Ministry of Trade, Industry & Energy (MOTIE), Republic of Korea (No. 20122010200071). M.-J. Park also acknowledges that this work was supported by the Human Resources Development of the KETEP grant funded by the Ministry of Trade, Industry & Energy (No. 20154010200820).

NOMENCLATURE

A : carbonator section [m^2]
C_{CO_2} : concentration of CO_2 [mol/m^3]
$C_{CO_2,e}$: equilibrium concentration of CO_2 [mol/m^3]
C_{in} : carbonator inlet concentration [mol/m^3]
E_{carb} : CO_2 capture efficiency in the carbonator
f_a : volumetric fraction of CaO that reacts in the fast rate regime
f_e : molar fraction of CO_2 at equilibrium under the reaction conditions
f_{in} : inlet molar fraction of CO_2
$F_{CO_2,in}$: inlet molar flow rate of CO_2 [mol/s]
e_{max} : maximum thickness of the $CaCO_3$ layer in the sorbent particle pores, 50 nm
k_s : kinetic rate constant [$m^4/mol/s$]
M_{CaCO_3} : molecular weight of $CaCO_3$ [g/mol]
M_{CaO} : molecular weight of CaO [g/mol]
N_{CaO} : number of moles of CaO held in the carbonator [kgmol]
r_{CaO} : carbonation rate of the active sorbent [s^{-1}]
r_{CO_2} : consumption rate of CO_2 [s^{-1}]
F_0 : sorbent make-up flow rate [mol/s]
F_R : sorbent circulating flow rate [mol/s]
S_N : reaction surface in the N cycle [m^{-1}]
t^* : characteristic time at which the carbonation rate becomes zero [s]
W_{CaO} : carbonator holding weight of CaO [kg]
X : conversion of sorbent particles in the carbonator
X_N : maximum conversion of sorbent particles in the N^{th} cycle

Greek Symbols

ρ : density [g/m^3]
τ : average residence time [s]
τ_{eff} : effective average residence time [s]

REFERENCES

1. M. Karl, T. Svendby, S. E. Walker, A. S. Velken, N. Castell and S. Solberg, *Sci. Total Environ.*, **527-528**, 185 (2015).
2. D. C. Ozcan, H. Ahn and S. Brandani, *Int. J. Greenhouse Gas Control*, **19**, 530 (2013).
3. T. Shimizu, T. Hirama, H. Hosoda, K. Kitano, M. Inagaki and K. Tejima, *Chem. Eng. Res. Des.*, **77**, 62 (1999).
4. D. A. Nemtsov and A. Zabaniotou, *Chem. Eng. J.*, **143**, 10 (2008).
5. K. Atsonios, P. Grammelis, S. K. Antiohos, N. Nikolopoulos and E. Kakaras, *Fuel*, **153**, 210 (2015).
6. A. Lasheras, J. Ströhle, A. Galloy and B. Epple, *Int. J. Greenhouse Gas Control*, **5**, 686 (2011).
7. J. Ylätalo, J. Ritvanen, B. Arias, T. Tynjälä and T. Hyppänen, *Int. J. Greenhouse Gas Control*, **9**, 130 (2012).
8. F. Fang, Z.-S. Li, Cai and S. Ning, *Energy Fuels*, **23**, 207 (2009).
9. S. Wang, H. Shen, S. Fan, Y. Zhao, X. Ma and J. Gong, *AIChE J.*, **59**, 3586 (2013).
10. B. Hejazi, J. R. Grace, X. Bi and A. Mahecha-Botero, *Fuel*, **117**, Part B, 1256 (2014).
11. A. Sarkar, W. Pan, D. Suh, E. D. Huckaby and X. Sun, *Powder Technol.*, **265**, 35 (2014).
12. K. Atsonios, M. Zeneli, A. Nikolopoulos, N. Nikolopoulos, P. Grammelis and E. Kakaras, *Fuel*, **153**, 371 (2015).
13. M. Ayobi, S. Shahhosseini and Y. Behjat, *J. Taiwan Inst. Chem. E.*, **45**, 421 (2014).
14. D. Kunii and O. Levenspiel, *Ind. Eng. Chem. Proc. Des. Dev.*, **7**, 481 (1968).
15. D. Kunii and O. Levenspiel, *Chem. Eng. Sci.*, **55**, 4563 (2000).
16. J. C. Abanades, E. J. Anthony, D. Y. Lu, C. Salvador and D. Alvarez, *AIChE J.*, **50**, 1614 (2004).
17. M. Alonso, N. Rodríguez, G. Grasa and J. C. Abanades, *Chem. Eng. Sci.*, **64**, 883 (2009).
18. D. K. Lee, *Chem. Eng. J.*, **100**, 71 (2004).
19. K.-Y. Yoo, D.-Y. Shin and M.-J. Park, *Korean J. Chem. Eng.*, **31**, 1532 (2014).
20. D. Alvarez and J. C. Abanades, *Ind. Eng. Chem. Res.*, **44**, 5608 (2005).
21. C. Cao, K. Zhang, C. He, Y. Zhao and Q. Guo, *Chem. Eng. Sci.*, **66**, 375 (2011).